Experimental study of flexural fatigue behaviour of cement paste at the microscale

Gan, Yidong; Zhang, Hongzhi; Zhang, Yu; Xu, Yading; Schlangen, Erik; van Breugel, Klaas; Šavija, Branko

DOI
10.1016/j.ijfatigue.2021.106378

Publication date
2021

Document Version
Final published version

Published in
International Journal of Fatigue

International Journal of Fatigue 151 (2021) 106378

Contents lists available at ScienceDirect

International Journal of Fatigue

journal homepage: www.elsevier.com/locate/ijfatigue

Experimental study of flexural fatigue behaviour of cement paste at the microscale

Yidong Gan [a,*], Hongzhi Zhang [b], Yu Zhang [a], Yading Xu [a], Erik Schlangen [a], Klaas van Breugel [a], Branko Šavija [a]

[a] Microlab, Faculty of Civil Engineering and Geosciences, Delft University of Technology, Delft 2628 CN, the Netherlands
[b] School of Qilu Transportation, Shandong University, Jinan, PR China

ARTICLE INFO

Keywords:
Flexural fatigue
Micro-cantilever bending
Cement paste
SEM
Viscoelasticity

ABSTRACT

This study presents an experimental investigation of fatigue properties of cement paste at the microscale. A strong size dependence is found for the flexural fatigue life of the cement paste specimen. Microscopic observations on the fractured surfaces suggest that there is a higher density of nano-scale cracks generated during the fatigue loading compared to the static fracture. However, the fatigue damage evolution is found to be very slow and small even under high stress levels. The development of residual deformation for cement paste can be explained by the combined effects of viscoelastic deformation and fatigue cracking growth.

1. Introduction

Fatigue is defined as a process of progressive, permanent change in the internal structure of the material [1,2]. The change in concrete is mainly attributed to the progressive growth of internal microcracks, which may eventually coalesce into macrocracks and lead to the complete fracture [3,4]. Generally, the fatigue failure in structural components occurs suddenly under cyclic load of magnitude much lower than their static loading capacity [4,5]. Moreover, hardly noticeable fatigue induced damage that accumulates over a long time could also deteriorate the durability of structures [6,7]. Many concrete structures, such as off-shore structures and bridges, are inevitably subjected to a large number of cyclic loadings [8–10]. Therefore, understanding the fatigue behaviour of concrete is of great importance for ensuring the safety and durability of these structures. However, the phenomenon of concrete fatigue is very complex as it inherently involves multiple spatial scales owing to the multiscale heterogeneous nature of concrete [11,12]. The concrete can be considered as a complicated system [13]. The presences of numerous pores and cracks ranging from sub-nanometres to centimetres, along with the wide scope of sizes of ingredients in concrete, lead to the complex mechanical interactions, i.e. fracture and crack propagation, at different scales [14]. To address the essential question of how the fatigue fracture process happening at finer scales affects the macroscopic fatigue performance of concrete, experiments and simulations are needed at every scale.

Over the past several decades, most of research efforts devoted on the concrete fatigue focused on the macroscale [2,10,15–19]. The empirical S-N curves (stress level versus fatigue life), based on extensive experimental results, remains the primary method to study the macroscopic fatigue performance of concrete due to its convenience for structure design. Some researchers have also modified the *S-N* approach by considering the probabilistic nature of concrete fatigue [8,20]. However, a clear and thorough understanding of fatigue fracture process at the finer scales is still missing. In a recent theoretical work of Le and Bažant [14], the nano-scale crack growth has been related to the macroscopic fatigue strength of quasi-brittle materials based on fracture mechanics. The authors have assumed that the propagation of nano-scale cracks is governed by the thermally activated breakage of atomic bonds or rupture of nano-particle connections [14,21,22]. The proposed theory yields a power-law relation for the stress-life curve, which agrees with the Basquin's law [23]. As for the scales between the nano- and the macro-scale, the microstructural mechanisms are believed to play an important role in the fatigue fracture process. At the mesoscale, concrete mainly comprises cement paste, various sizes of aggregates and the interfacial transition zone (ITZ) between them. When subjected to the fatigue loading, it is found that the pre-existing cracks situated mostly in the regions of ITZ would propagate first and then coalesce with the fatigue cracks in the cement paste matrix [24–31]. Even though both the ITZ and matrix are experiencing the fatigue damage, the fatigue crack

* Corresponding author.
E-mail addresses: y.gan@tudelft.nl (Y. Gan), hzzhang@sdu.edu.cn (H. Zhang), Y.Zhang-28@tudelft.nl (Y. Zhang), Y.xu-5@tudelft.nl (Y. Xu), Erik.Schlangen@tudelft.nl (E. Schlangen), K.vanBreugel@tudelft.nl (K. van Breugel), B.Savija@tudelft.nl (B. Šavija).

https://doi.org/10.1016/j.ijfatigue.2021.106378
Received 17 March 2021; Received in revised form 6 May 2021; Accepted 3 June 2021
Available online 6 June 2021

Nomenclature

a, b	experimental coefficients for Wöhler fatigue equation
$C(t)$	fatigue compliance
d	fractured length
E_{static}	static elastic modulus
f_t	flexural strength
F_{max}	maximum fatigue load
h	side length of the square beam cross-section
I	moment of inertia
k	slope of load–displacement curve
L	the loading length of beam
N	number of cycles
S	stress level
S_{nom}	nominal stress levels
S_{mod}	modified stress levels
t_i	time at the i-th step
α, β	two creep parameters
$\varepsilon(t)$	strain for the upper fibre of beam at the fixed end
ε_{ve}	viscoelastic strain
σ	stress
σ_{max}	applied maximum stress
δ	displacement of the indenter tip

growth in ITZ seems to be faster than that of cracks in matrix. The effects of some meso-scale features, such as the aggregate type, air content and properties of pastes, on the fatigue performance of concrete have been investigated by several researchers [15,24–27,29–33]. It is clear that the meso-structure of concrete and local mechanical properties of its constituents, including both static and fatigue properties, have strong influences on the global fatigue performance. Whereas the mesoscale fatigue behaviour of concrete has been extensively studied in recent years, the available data concerning the fatigue behaviour of cement paste at the microscale is rather scarce. Since the cement paste is the binding phase in concrete, the knowledge regarding the microscopic changes of cement paste subjected to the fatigue loading is also important for fatigue analysis of concrete and requires deeper understanding.

To fill the aforementioned knowledge gap, the fatigue bending tests on the micro-cantilever beams (MCB) of cement paste developed by the authors [34–36] are carried out. The fatigue properties of cement pastes in terms of fatigue life, stiffness degradation and residual deformation development are studied. A comparison of static and fatigue fractured surfaces by means of the microscopic observation is performed. X-ray computed tomography (XCT) technique is also used to assess the fatigue damage accumulation of cement paste. General discussions regarding the evolutions of fatigue damage and residual deformation are also provided.

2. Materials and methods

2.1. Materials and experimental procedure

2.1.1. Materials

Cement pastes with w/c ratio of 0.4 and 0.5 were prepared using standard grade CEM I 42.5 N Portland cement (ENCI, the Netherlands) and deionized water. The Blaine fineness of cement is 2840 cm^2/g (provided by the manufacturer). The pastes were first cast in plastic cylindrical moulds with 24 mm diameter and 39 mm height. The fresh paste was rotated at a speed of 2.5 rpm for 24 h at room temperature (20 °C) to prevent bleeding. The samples were cured under sealed conditions at room temperature for 28 days. After demoulding, the hardened cement pastes were cut into slices with the thickness of 3 mm. The slices were then immersed in isopropanol to arrest the hydration [37].

2.1.2. Preparation of micro-cantilever beams

Micro-cantilever beam (MCB) specimens were prepared using a precision micro-dicing machine (MicroAce Series 3 Dicing Saw), which is generally used to cut semiconductor wafers. Firstly, cement paste slices were ground to obtain two smooth and parallel surfaces using a Struers Labopol-5 thin sectioning machine. In this grinding process, two grinding discs of 135 μm and 35 μm were used in sequence. The thickness of each slice was controlled at 2150 μm. Afterwards, two perpendicular cutting directions with the same cutting spacing were applied on the samples using the micro-dicing machine. In this way, multiple rows of cantilever beams with a square cross section of 300 μm × 300 μm were generated. The cutting depth, i.e. the cantilevered length, was approximately 1650 μm ± 10 μm. The cutting process is schematically shown in Fig. 1.

The cross-sections of several beams have been examined by using an Environmental Scanning Electron Microscope (ESEM), see Fig. 2. No cracking as a consequence of the cutting process has been observed. An overall accuracy of the cross-sectional dimensions of ±1.5 μm can be reached with this fabrication process. Precautions have also been taken to minimize the carbonation of the samples before testing by storing the beams in isopropanol.

2.2. Quasi-static and fatigue bending test

2.2.1. Experimental set-up

Quasi-static and fatigue tests were performed using a KLA Nano-indenter G200. The Nano-indenter was equipped with a cylindrical wedge indenter tip with a length of 200 μm (Fig. 3). It was used to apply vertical line loads at the free end of the MCB. Before testing, the angle and centre of the tip were calibrated by probing into a standard aluminium reference sample. The baseplate of MCB was attached on a metal surface using cyanoacrylate adhesive, and the angle of beam was carefully adjusted under the in-situ microscope in the nanoindenter to ensure that the line load is applied perpendicular to the beam longitudinal axis. The experimental set-up is schematically shown in Fig. 4. Before starting the test, the coordinates of the loading position and the fixed end were recorded under the microscope to determine the loading length L of each beam. All tests were conducted in a well-insulated chamber preventing any significant change of temperature and RH. The average temperature and RH during the tests were 26.1 ± 0.6 °C and 34.4% ± 0.7%. Prior to the tests, the samples were kept in the chamber for temperature equalization until the thermal drift rate was below 0.05 nm/s.

2.2.2. Quasi-static bending test

Before fatigue testing, the mechanical properties of MCBs, i.e. flexural strength and static elastic modulus, should be determined. For each w/c ratio, 30 cantilever beams were monotonically loaded to failure. The loading procedure was displacement-controlled with a constant loading rate of 50 nm/s. The load and displacement responses were measured by the Nano-indenter. In general, a major crack initiates near the fixed end of beam during the loading, which eventually leads to complete fracture of the beam. After the static failure, the coordinates of the fracture point were also recorded to determine the fractured length d of each beam. The maximum load F_{max} and slope of load–displacement curve k (in the range between 40% and 60% of the maximum load) during loading are respectively used to determine the flexural strength f_t and static elastic modulus E_{static} according to the classical beam theory [34,35,38]:

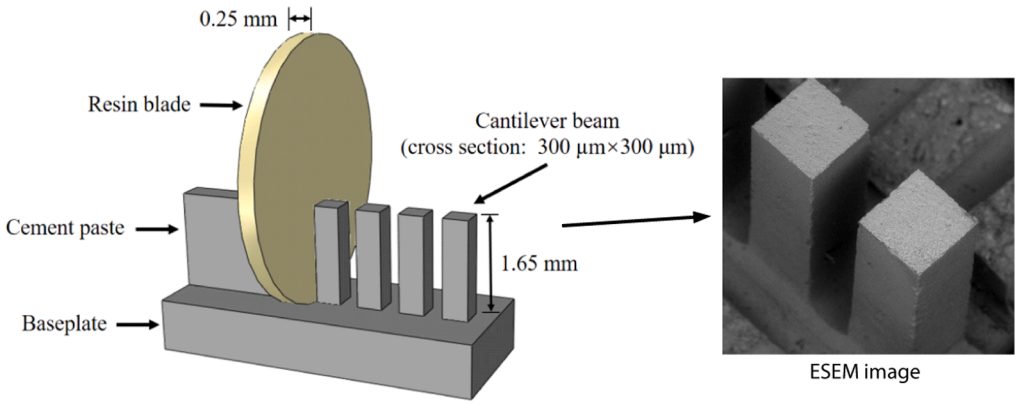

Fig. 1. Schematic diagram of sample preparation [34].

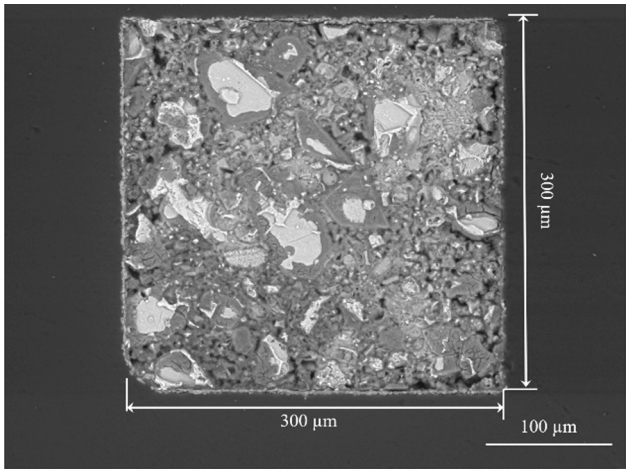

Fig. 2. Backscattered electron image of the cross-sections of MCB with w/c 0.4.

$$f_t = \frac{F_{max} dh}{2I} \quad (1)$$

$$E_{static} = \frac{kL^3}{3I} \quad (2)$$

where d is the fractured length, h is the side length of the square beam cross-section, and $I = h^4/12$ is the moment of inertia. Since one end of the cantilever beam is not perfectly fixed, there will be some additional displacement under loading due to the deformation of baseplate and the adhesive layer. By using the finite element method [34], it was found that the deformations of the baseplate and the adhesive layer account for $14 \pm 0.2\%$ and $0.5 \pm 0.1\%$ of the total displacement, respectively. These additional displacements will be excluded from the determination of the elastic modulus. In order to validate the experimental protocol, five glass cantilever beams were fabricated and tested. The measured average elastic modulus of glass beams through bending tests is 69.1 ± 1.2 GPa, which has been calibrated using the value 14.5%. For comparison, the conventional nanoindentation technique equipped with a Berkovich tip was used to measure the indentation modulus of glass. In total, 10 indents were performed, and the measured average indentation

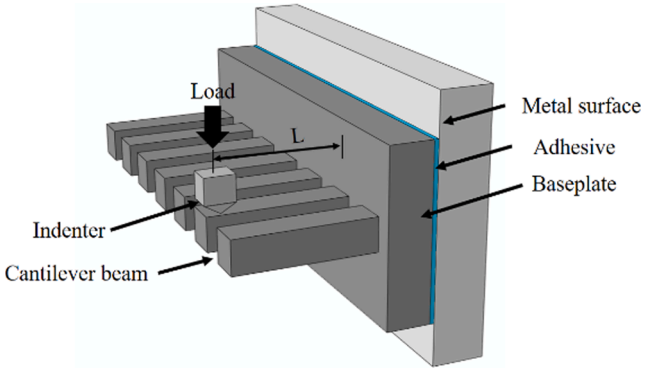

Fig. 4. Schematic diagram of test set-up [35].

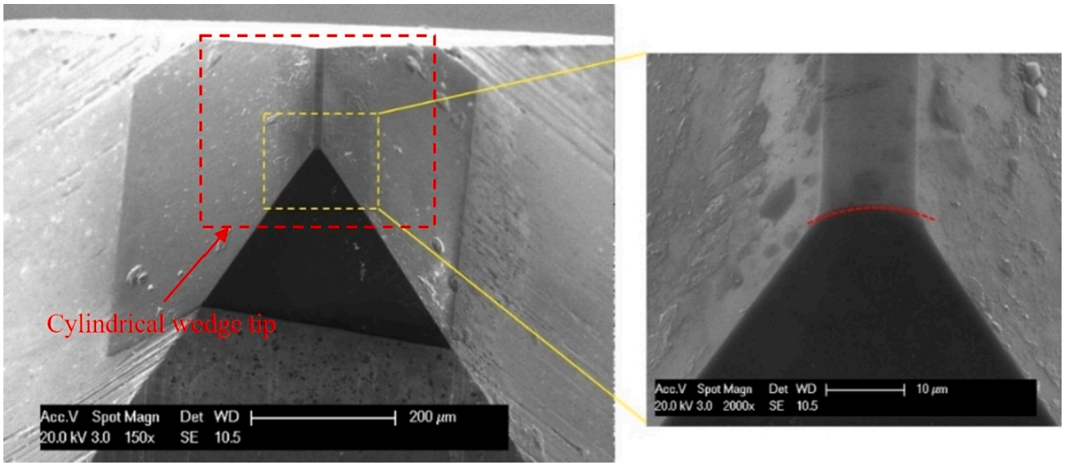

Fig. 3. Secondary electron image of the diamond cylindrical wedge tip with an enlarged view of the tip head [35].

modulus is 70.1 ± 1.8 GPa, which is very close to the result obtained in bending tests. Therefore, the methods of testing and results interpretation used in the current paper can be considered reliable.

2.2.3. Fatigue bending test

The fatigue bending tests were carried out under load control. The cyclic loads were applied in the form of triangular loads with a constant amplitude at a loading frequency of 0.55 Hz, see Fig. 5. For each value of the w/c ratio, 30 MCBs were tested under different loading levels. For w/c 0.4 series, the maximum loading level ranges from 50 mN to 70 mN corresponding to around 75–95% of static flexural strength, and the minimum loading level is kept around 1.5–2.1 mN. The maximum loading level of w/c 0.5 series varies from 35 mN to 50 mN, which corresponds to approximately 70–95% of static flexural strength. The minimum loading level for this series is around 1.0–1.5 mN. The stress ratio R between minimum and maximum cyclic load was kept equal to 0.03. During the fast loading–unloading regime, the loading magnitude is not perfectly controlled by the Nano-indenter. Small disturbances (2–5% of loading amplitude) for both upper load and lower load were observed. Therefore, the recorded actual loading level was used for the determination of stress level. Before each fatigue test, the MCB was preloaded to the maximum load and completely unloaded to reduce the possible plastic deformation generated under the indenter tip.

Due to the technical limitation of the testing duration of the used nano-indenter, the fatigue testing procedure was separated into multiple cycle blocks with identical loading procedure. Each cycle block contains 500 loading–unloading cycles and is automatically conducted in succession with a very short rest period (around 100 s). The beam is completely unloaded after finishing one cycle block and then reloaded for the next cycle block. Run-out tests were stopped at the limit of 200,000 cycles. At the end of each fatigue test, the nano-indenter will apply a constant low load with around 0.01% of maximum load to measure the drift rate and automatically calibrate the displacement responses. However, most of the measured drift may be affected by the viscoelastic recovery because of the viscoelastic nature of cement paste [39]. Therefore, the calculated drifts were deducted from the calibrated total time-dependent displacements for all tests. Many researchers found that the deformation of cementitious material exhibits a three-stage behaviour, which can be used to quantify the development of fatigue damage [9,40–43]. Fig. 6 presents the typical displacement-cycles number curve of MCB. Overall, the displacement evolution can also be divided into three stages: the first stage is unstable and comparatively transient, which occupies only 1–2% of the total loading procedure. With the proceeding of cyclic loading, displacement evolution curve turns into a stable stage, which covers around 99% of the whole test duration. In the third stage, the displacement grows rapidly within a few cycles until the MCB suddenly fails, which results in an overshoot of the indenter tip, as is shown in Fig. 6.

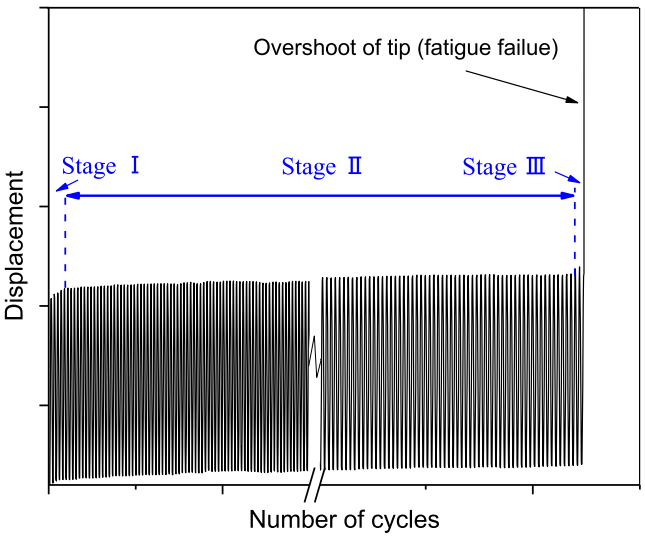

Fig. 6. Typical displacement-cycles number curve.

Another important characteristic investigated in most fatigue studies is the increase of the strain at the maximum or minimum loading level during the loading cycles [9,40–42,44]. In this study, the change of strain at the maximum loading level is defined as the residual strain, and the fatigue compliance $C(t)$ was defined by dividing the residual strain by the half of the applied maximum stress ($\sigma_{max}/2$). For each MCB, the time-dependent strain $\varepsilon(t)$ at the upper fibre of the fixed end and the corresponding fatigue compliance were calculated based on the classical beam theory:

$$\varepsilon(t) = \frac{3\delta h}{2L^2} \tag{3}$$

$$C(t) = \frac{2\varepsilon(t)}{\sigma_{max}} \tag{4}$$

where δ is the measured displacement of the indenter tip. Fig. 7 gives us the typical development of residual strain at the upper fatigue load. For each individual cycle block, after a few cycles (initial stage) the residual

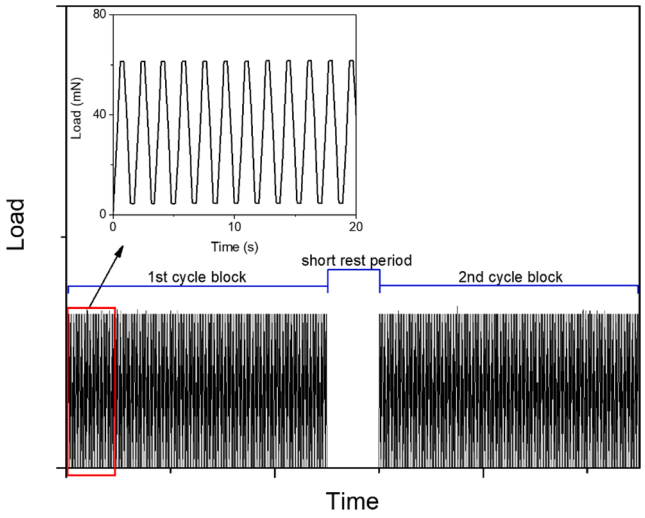

Fig. 5. Cyclic load history applied in MCB fatigue tests.

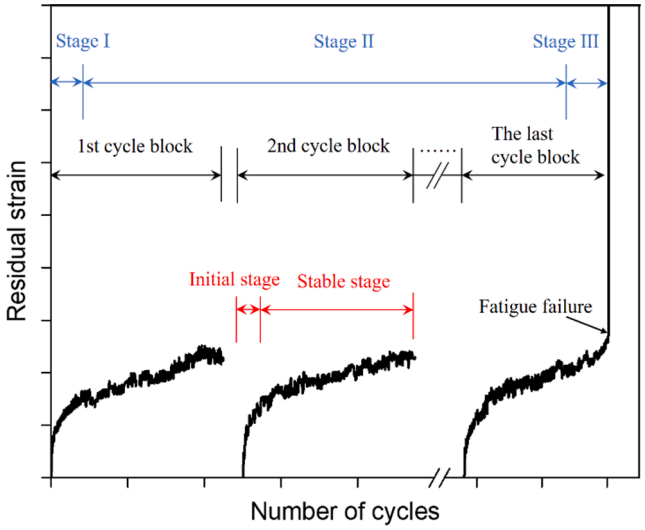

Fig. 7. Typical development of residual strain at the upper fatigue load.

strain development turns into a stable stage. Only in the last cycle block, the residual strain starts to increase rapidly before the fatigue failure. For each MCB, the residual strain and the corresponding fatigue compliance of each cycle block at the second stage have been calculated and averaged.

Attempts have also been made to assess the fatigue damage inside the cement paste by using the non-destructive X-ray computed tomography (XCT) technique [45,46]. As is shown in Fig. 8, the region of interest (ROI) in the initial microstructure of MCB, i.e. the local region near the fixed end of beam with the size of 300 × 300 × 600 μm^3, was first scanned before the fatigue test. The scanned MCB was then subjected to the cyclic loadings up to 200,000 cycles with the stress level of 90%. Afterwards, the damaged sample was scanned again to evaluate the possible fatigue damage. After acquiring the grey-value based XCT images, the pore segmentation was conducted using the global threshold method [47]. Three extra intact beams for each w/c ratio were also scanned and segmented to determine the total porosity. The X-ray source tube was set at 90 kV/100 μA during scanning, resulting in a voxel resolution of 0.5 × 0.5 × 0.5 μm^3 (see Fig. 8).

3. Experimental results and discussion

3.1. Mechanical properties measured in quasi-static tests

A typical load-displacement curve of MCB (w/c 0.4, 28d) under monotonic loading is shown in Fig. 9. The static mechanical properties as well as porosities of cement pastes measured by XCT for both w/c ratios at the age of 28 days are summarized in Table 1. As was expected, a lower w/c ratio leads to higher elastic modulus and strength, mainly owing to the decreased porosity. Note that pores smaller than the image resolution (i.e. 0.5 μm) cannot be detected by XCT, and are mixed within the segmented solid phases. Therefore, the porosity measured by XCT is much lower than the result of the mercury intrusion porosimetry (MIP) [48]. Nevertheless, the difference in porosity for different w/c ratios is clear. When the measured elastic moduli are plotted against flexural strengths in Fig. 10, a general positive correlation between these two properties can be observed for both w/c ratios. Due to the highly heterogeneous nature of cement paste at the microscale, the results exhibit a wide variation, as was expected [34,35]. More specifically, the local spatial distribution of pores and hydration products at the fixed end of beam may largely affect the strength of MCB, while the whole microstructure of MCB accounts for the variation of elastic modulus. The relationship obtained in Fig. 10 will be used in the analysis of fatigue results.

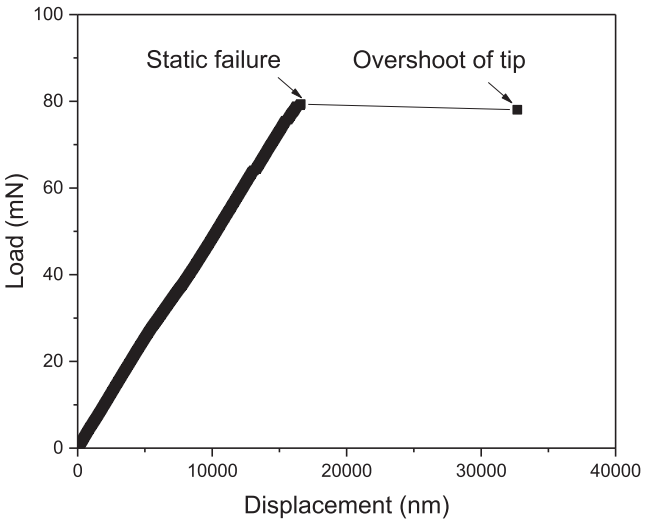

Fig. 9. Typical load–displacement curve of MCB (w/c 0.4, 28d) under monotonic loading.

Table 1
Measured porosities and mechanical properties of MCBs (28d).

w/c ratio	Porosity measured by XCT	E_{static} (GPa)	f_t (MPa)
0.4	7.40% ± 0.43%	15.09 ± 2.06	24.23 ± 2.90
0.5	12.06% ± 0.75%	10.19 ± 2.46	19.47 ± 4.38

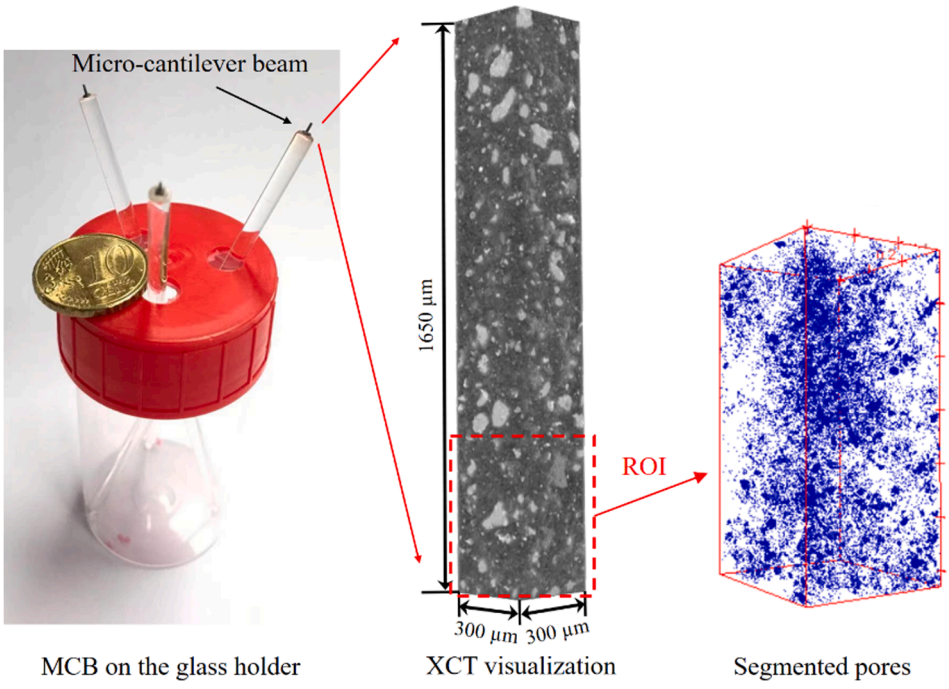

Fig. 8. The CT scanning of the micro-cantilever beams and segmented pore structure.

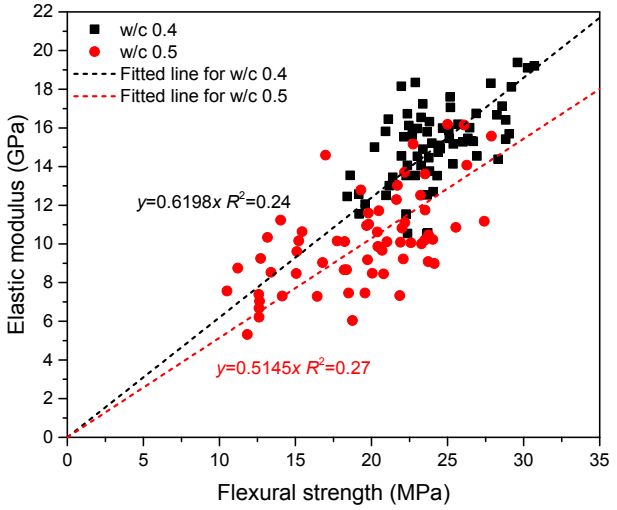

Fig. 10. The relationship between the elastic modulus and flexural strength (28d).

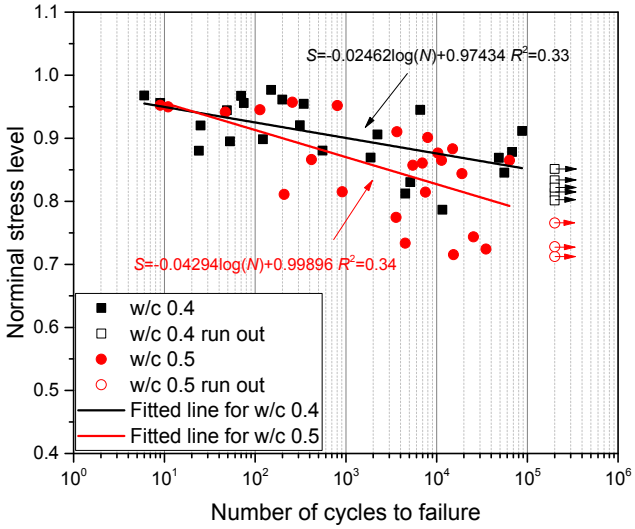

Fig. 11. The nominal stress level versus number of cycles to failure.

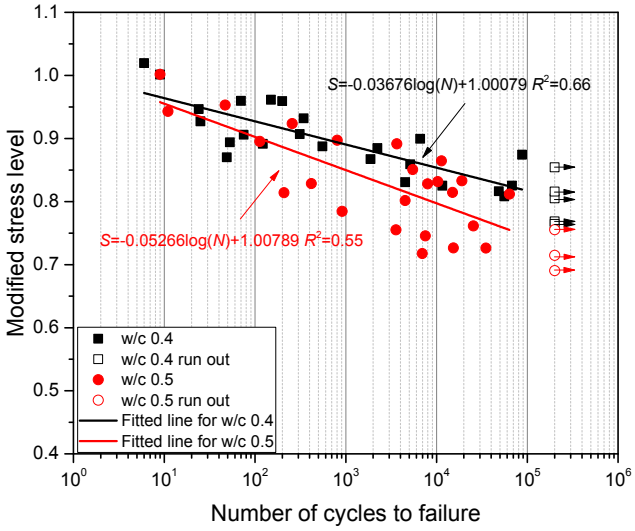

Fig. 12. The modified stress level versus number of cycles to failure.

3.2. Fatigue life and S-N curves

Fatigue behaviours of materials, both from a scientific and engineering perspective, are normally described by the so-called *S-N* curves. In this diagram, a (linear) relationship is usually found between the logarithm of the number N of cycles and the maximum fraction of the strength, i.e. stress level S. This relationship is known as the Wöhler fatigue equation [10], and is given by:

$$S = a \cdot \log(N) + b \tag{5}$$

where a and b are experimental coefficients. Note that there is another fatigue equation [4,15,49], which considers the ratio of minimum fatigue stress to the maximum fatigue stress. Since this stress ratio was kept low and constant (i.e. 0.03) for each fatigue test, the fatigue equation Eq. (5) is adopted in current study. In general, the average strength measured in static tests is used to determine the nominal stress level for fatigue experiments. This engineering approach is used for convenience, as negligible variation of sample strength is expected at the macroscale. However, despite the huge scatter inevitable in fatigue tests, the large variations of mechanical properties at the microscale may undermine the correctness and practicality of this method. To consider the individual variation of strength of each MCB, the initial elastic modulus (determined by the slope in the range of 40–60% of strength) measured before the fatigue test was used to predict the strength based on the linear correlation obtained in Fig. 10. Although the correlation is far from perfect, this allows to reduce the scatter originating from the variation of material properties. One should also note that, in comparison to quasi-static testing at lower strain rates, the accelerated cyclic loading tests with faster loading rates may lead to higher flexural strengths due to the strain rate sensitivity of cementitious materials [50–53]. As a consequence, the calculated stress levels are likely to be artificially higher than those 'true' stress levels determined as a function of static strengths measured at strain rates equivalent to the loading rate during the fatigue tests. Nevertheless, these stress levels determined in this study are only used as guidelines. For comparison, both the nominal stress levels S_{nom} using the average strengths measured in previous quasi-static tests and the modified stress levels S_{mod} considering individual sample strength, which is based on elastic modulus, have been calculated.

The *S-N* curves using the nominal and modified stress levels are shown in Fig. 11 and Fig. 12. Based on the least square method, linear regression analyses were carried out to determine the Wöhler equation, i.e. Eq. (5). In Fig. 11, it is difficult to find a general trend when the nominal stress level is used. The fatigue life for the same nominal stress level is rather scattered at the microscale, as is indicated by the low coefficients of determination (R^2). The results in Fig. 12 show relatively high coefficients of determination after the variation of strength for individual sample is considered. Even though the value of R^2 is still low, it is very typical for fatigue results and it seems difficult to consider all the sources of scatter. For all modified stress levels (S_{mod}), the fatigue life of w/c 0.4 sample is generally higher than that of w/c 0.5 sample.

It has been reported that the fatigue performances of quasi-brittle materials in terms of fatigue life and crack growth rate are strongly dependent on the specimen size [14,22,31,54–60]. When the results obtained here are compared to the macroscopic fatigue results of cement paste in the literature [61,62], it is found that, given the same nominal stress level, the fatigue life of cement paste at the microscale is apparently longer. For instance, at the nominal stress level of 80%, the number of cycles to failure for cement paste subjected to compressive cyclic loading at the macroscale lies in the range of 10^2-10^4 [61–63], which is almost two orders of magnitude lower than the flexural fatigue life of MCB at the microscale. For stress levels lower than 80%, the difference in fatigue life becomes larger. Note that the compressive fatigue resistances of cementitious materials are found to be slightly higher than

their tensile fatigue resistances at the same stress levels [64], while it is also suggested in [10] that similar *S-N* equations can be used for both compressive and flexural fatigue.

Moreover, it has been widely reported that the fatigue life of cementitious materials decreases with decreasing loading frequency [40,49,65]. Herein, the MCBs were subjected to the cyclic load with loading frequency of only 0.55 Hz, which is much lower than the commonly used frequency in macroscopic tests (5–10 Hz) [40,49,65,66], but they still exhibit longer fatigue life. It should be also pointed out that, if one considers the absolute magnitude of the stress, the number of cycles to failure at a particular stress is much higher for the small size sample than for the large size sample [31] as the strengths of cement-based materials are also size-dependent [67,68]. The fatigue size effect of quasi-brittle materials was first demonstrated in the works of Bažant and co-workers [55,56] and has recently been tested and analysed in [54]. The fatigue crack growth rate, specifically referred to the Paris law coefficient, is found to exhibit a substantial size effect, analogous to the size effect of fracture under monotonic loading [54]. In other words, the fatigue damage evolution becomes slower for smaller samples and, consequently, the fatigue life tends to increase with the decreasing sample size [31,54,55]. In contrast to normally used laboratory-scale cement paste samples, the MCBs at the microscale do not contain initial defects with larger sizes, like meso-cracks and air voids (>300 μm), which could eventually reduce the overall fatigue resistance [69]. Furthermore, due to the extremely thin cross-section of MCB, very low moisture gradients would be expected before and during the testing. This may result in a lower degree of shrinkage-induced eigenstresses compared to larger samples, which could also give rise to the better fatigue performance [26]. However, it should be mentioned that the low RH used in current study may also increase the potential of cracking due to the large drying shrinkage.

3.3. Evolution of fatigue damage

It has been recognized that the cement-based materials under fatigue loading experience progressive damage accumulation, which is mainly attributed to the initiation and propagation of microcracks [30,70]. In general, the gradual development of fatigue damage causes a steady decrease in the stiffness of the material [71]. Therefore, the degradation of stiffness can be used as an indicator of fatigue damage evolution. By contrast, the direct examination of microstructure through XCT technique could also help to reveal the possible growths of microcracks. In this study, both approaches were attempted to characterize the fatigue damage.

3.3.1. Changes in MCB stiffness

The stiffness of MCB is determined by the slope of the ascending load–displacement curve under cyclic loading. For each w/c ratio, the variations of stiffnesses for 10 MCBs with the highest nominal stress levels were normalized to the initial stiffness (k_{int}) and plotted against the normalized number of cycles in Fig. 13. Despite small fluctuations, the stiffnesses of most samples slightly decreased with cycles during the whole fatigue life, and some of them even remained almost unchanged before the fatigue failure. The average reduction percentage in stiffness before failure is calculated as 2.76 ± 1.31% for w/c 0.4 samples and is 4.01 ± 3.06% for w/c 0.5 samples. Unlike most macroscopic fatigue results of mortar or concrete samples [40,71,72], where distinct stiffness degradations of around 10–40% were observed and damage generated mainly at the interfacial transition zone (ITZ), the cement paste at the microscale seems to experience very slow and limited damage accumulation during most of the fatigue life. Once nano- or microcracks nucleate and form a major crack under cyclic loading, the MCB immediately fails. It turns out that a very small degree of fatigue damage is sufficient to cause a complete fatigue failure of MCB. Note that slight increases in mechanical properties of concrete samples after fatigue tests have also been reported in the literature [43,72,73]. This phenomenon

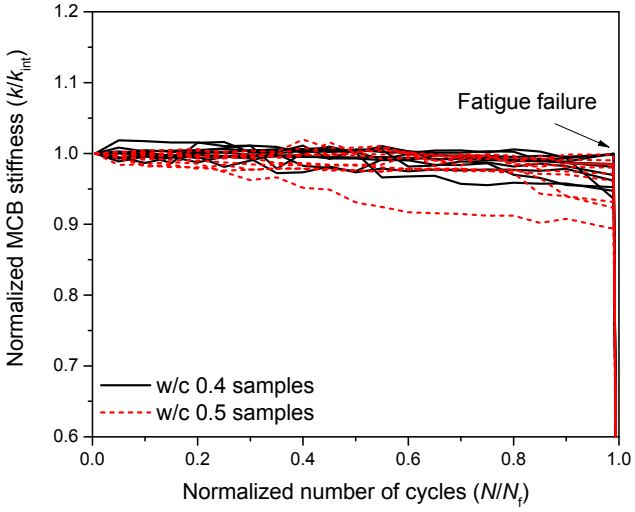

Fig. 13. Stiffness degradations of 10 MCBs (28d) for each w/c ratio under cyclic loading (note that vertical axis does not start at zero).

may be attributed to possible strengthening mechanisms such as the consolidation or compaction of cement paste or relief of eigenstress in the regions surrounding the cracks under cyclic loading. These effects may also account for the observed low stiffness degradations of MCBs. Since the remaining strengths of run-out MCBs were not measured after fatigue tests, these possible strengthening mechanisms cannot be verified in the current research.

3.3.2. Fatigue damage evaluation through XCT

XCT observations were carried out on a group of MCBs. Owing to the large scatter of fatigue results, accurate prediction of fatigue life and damage monitoring at the microscale are extremely challenging. As a result, several samples have failed before the second scanning (200,000 cycles). Nevertheless, the two remaining samples (w/c 0.4) were scanned and analysed. The fatigue damage evaluation through XCT is schematically shown in Fig. 14. After the pore segmentation, the average porosity of ROI changed from 7.72 ± 0.45% to 7.80 ± 0.38%. It appears that the porosities measured by XCT are almost identical for original and damaged samples. This may suggest that most of fatigue damage was formed at much smaller length scale, at least lower than XCT resolution (i.e. 0.5 μm), which cannot be detected by the XCT. While for concrete samples the fatigue damages at the later stage are often visible and can be clearly identified using XCT [46,71,74,75] as significant number of cracks with large cracking widths are generated near the ITZ. The fatigue damage in cement paste could be in the form of cracking and propagation at the nanoscale or associated with separations between nano-gel particles of the calcium silicate hydrate [14]. Therefore, the XCT with limited resolutions may not be an appropriate approach to capture the minor fatigue damage of cement paste at the microscale. More sensitive non-destructive techniques, such as electrical resistivity measurement [76], dual-CT approach [77] and ultrasonic pulse attenuation [78], could be useful in this case. However, the difficulty in setting up the small-scale measurement would become another challenging technical mission.

3.4. ESEM analysis of fracture surface

For a better insight into the fatigue failure, ESEM image analyses were performed to study the fractured surfaces of MCBs after static and fatigue failure. The fractured beams were examined using both secondary electron (SE) and backscattered electron (BSE) modes in an ESEM. Fig. 15 compares the BSE and SE images of the typical static and fatigue fracture surfaces of MCBs at the magnification of 500×. At a first

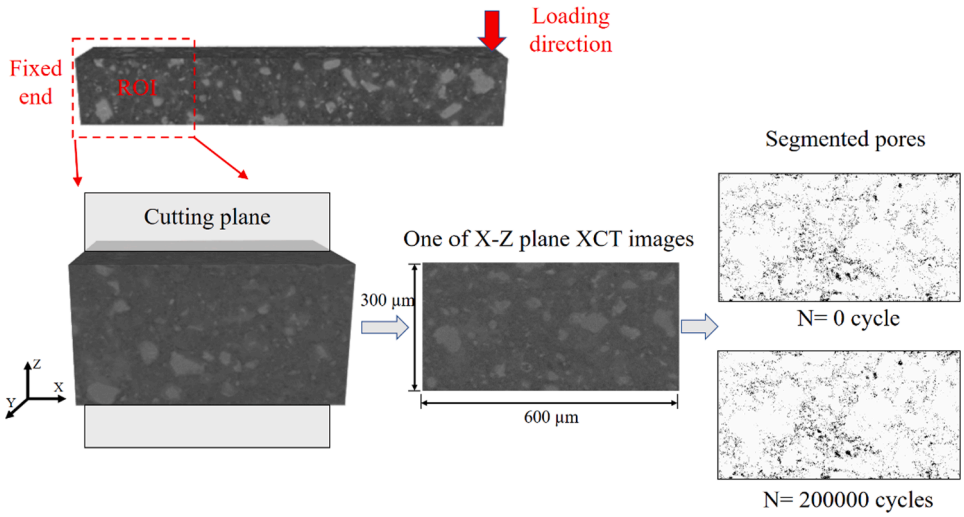

Fig. 14. XCT examination of fatigue damage in MCBs (w/c 0.4).

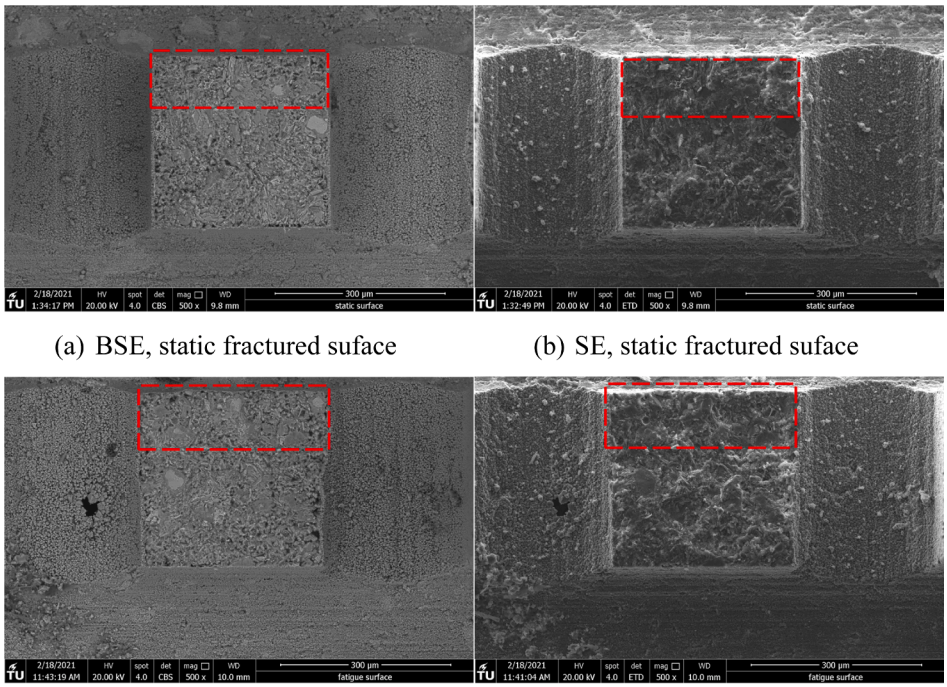

(a) BSE, static fractured suface (b) SE, static fractured suface

(c) BSE, fatigue fractured suface (d) SE, fatigue fractured suface

Fig. 15. The overview of static and fatigue fractured surfaces (w/c 0.5).

glance, the overall difference between the static and fatigue fracture at this magnification is not obvious. It is known that the critical crack under flexural loading is most likely to initiate and propagate in the tensile zone of the cross-section (marked as red box in Fig. 15). Therefore, particular attention was paid on these areas, as is shown in Fig. 16 and Fig. 17.

Based on the BSE and SE images, multiple phases can be identified in the cement paste at the microscale, such as calcium hydroxide (CH), ettringite and calcium-silicate-hydrate (C-S-H). Moreover, some small cracks can also be found from these images at higher magnifications. The detected small cracks were marked for static and fatigue fractured surfaces (w/c 0.5) and presented in Fig. 18 and Fig. 19, respectively. Compared with the static failure samples, a higher density of cracks can be observed in fatigue fracture surfaces. Most of these small cracks are found in the fractured C-S-H phases, which are generally distributed around the stiff particles (e.g. unhydrated cement particle and CH) or near the pores. More importantly, most of them are nano-scale cracks and have the crack widths less than 500 nm, as is shown in Fig. 19. Note that a few observed fractures of CH (see Fig. 17, near the neutral axis of the cross-section of beam) are believed to be caused by the unstable cracking behaviour at the final stage of fatigue tests. It is then suggested that, under the fatigue flexural loading, fatigue damages in the form of multiple nano-cracks were generated and developed at the tensile zone of the cantilever beam. The fatigue crack growth behaviour at the nanoscale may be associated with the rupture of connections of C-S-H gel particles [14]. The slow stiffness degradation might be attributed to the accumulation of these minor damages. Furthermore, the randomly distributed nano-cracks with a relatively higher density could also explain the large scatter of the fatigue life to a certain degree as any small crack has the potential to develop into the primary crack, which

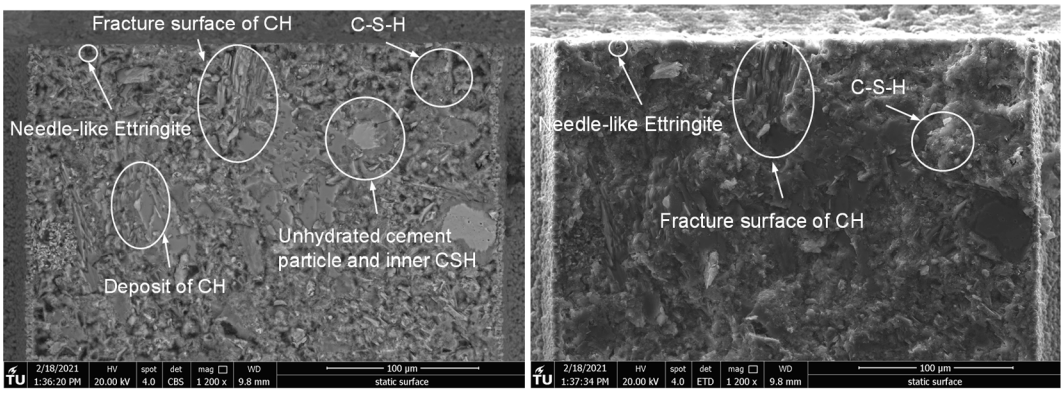

Fig. 16. The (a) BSE image; (b) SE image of tensile zone of MCB after static failure (w/c 0.5).

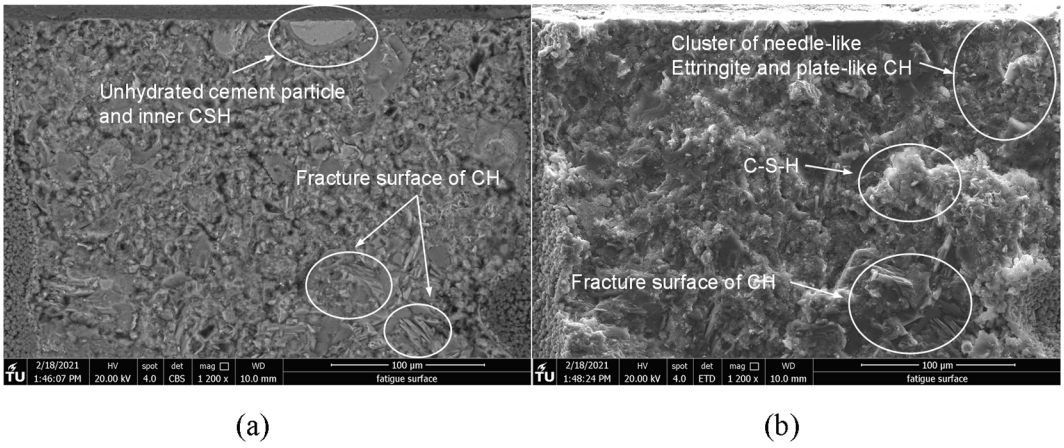

Fig. 17. The (a) BSE image; (b) SE image of tensile zone of MCB after fatigue failure (w/c 0.5).

results in the final fracture. By contrast, there are much fewer small cracks propagating during the monotonic flexural loading. This is also in accordance with the findings reported in [14,22,55], where much larger fracture process zones (FPZ) were measured in fatigue tests compared to the static tests. In several fatigue studies reported in the literature [4,79], some traces of "friction" were found on the fatigue fractured surfaces. Several researchers believe that the dissipative mechanisms in terms of the internal sliding and friction between the cracking surfaces are the main sources of fatigue damage evolution [80,81]. However, this kind of damage could not be detected in the ESEM images with current magnifications, and is possibly not significant in flexural fatigue tests.

The combined XCT and ESEM observations indicate that the apparently sound material before the fatigue failure has already been damaged. The nanoscale fatigue crack growths in the C-S-H phases could explain the limited stiffness degradation of MCBs. Since it is currently not possible to trace all the local sub-microscopic damages, a more appropriate approach is to consider fatigue as an essentially statistical effect of happenings on a nano-scale as is suggested in [20].

3.5. Development of fatigue compliance

Fig. 20 displays the typical fatigue compliance evolution of MCB subjected to multiple cycle blocks. It can be seen that the fatigue compliances increase with the cycles showing two distinct stages and they are similar for different cycle blocks. Despite the discontinuity between each load block, the development of residual displacement shows an overall increasing trend with nearly the same slope. It is documented in the literature that the first stage is characterised by a rapid increase of deformation, which is generally believed to be caused by the initiation and propagation of initial material defects like microcracks and pores [5,9,18,40,41,65,66]. The second stage presenting an almost linear increase of deformations is explained by the consequence of the stable crack growth [5,18,25,65,66,82]. This stable growth of deformation at the second stage, which occupies almost 95% of fatigue life, depends on the amplitude of the stress intensity factor near the crack tip [14,22,54]. The third stage before fatigue failure, which is shown in Fig. 7, always shows a dramatic increase in deformation due to an unstable crack growth. However, as has been previously examined by the stiffness evolutions and XCT observations of MCBs, the fatigue damage of cement paste at the microscale seems to be very small and slow. The linearly increased deformation at the second stage cannot be explained solely by the minor damage accumulation. The cyclic creep, or so-called fatigue creep, must be involved in the fatigue deformation of cement paste due to the visco-elastic/plastic nature of C-S-H [9,35,83–85]. Note that the term 'creep' used here is mainly referred to the time-dependent deformation behaviour of C-S-H [86,87]. It has been suggested in [9] that the residual strain of concrete in the first stage is mainly caused by the cyclic creep effect, while the coupling of cyclic creep and fatigue damage determines the irreversible strain accumulation in the second stage [9,83].

In order to examine the viscoelastic deformation of cement paste under the cyclic loading, the Boltzmann superposition principle (BSP) is here adopted [88]. This principle allows the calculation of linear viscoelastic deformation of a material subjected to arbitrary stress history by assuming an independent response to any given load. The basic

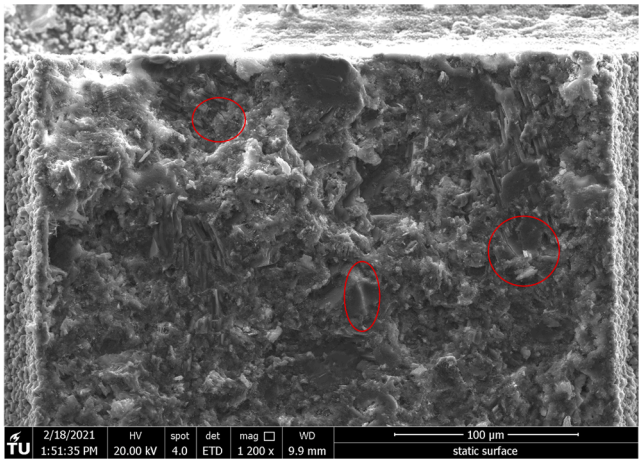

(a)

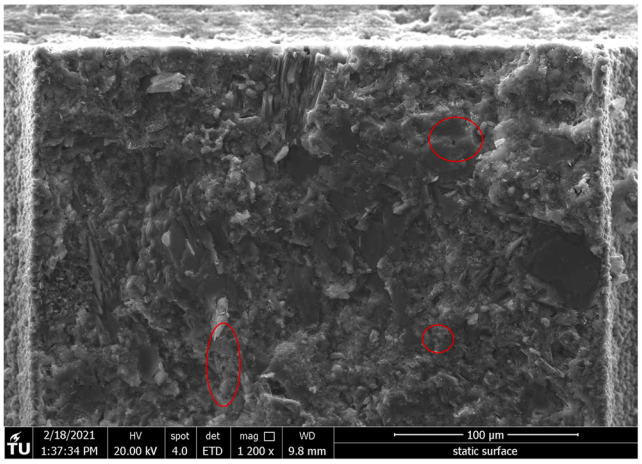

(b)

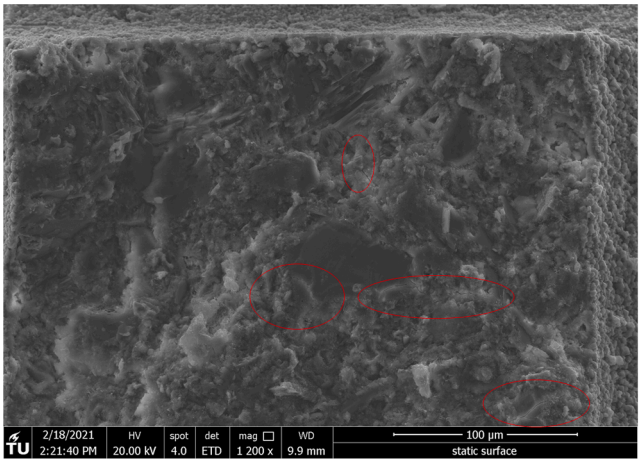

(c)

Fig. 18. Three static fractured surfaces of MCBs and marked cracks.

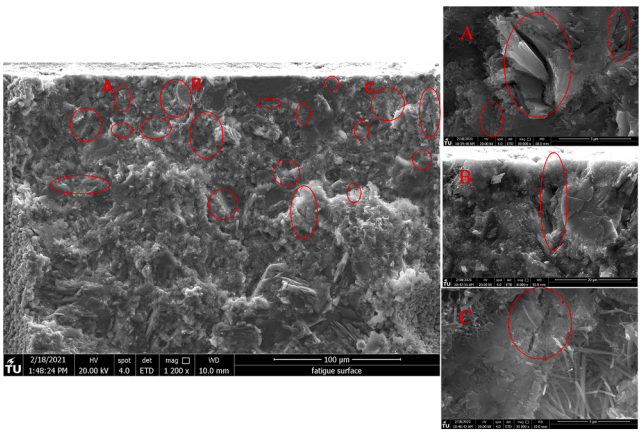

(a)

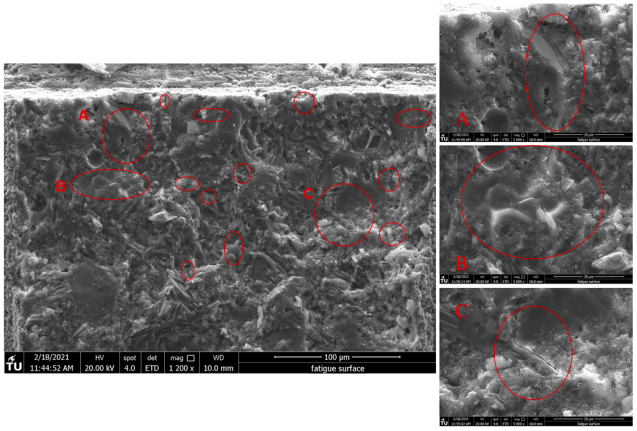

(b)

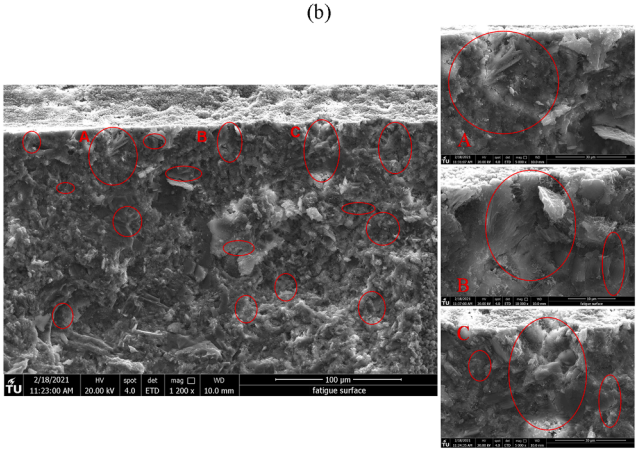

(c)

Fig. 19. Three fatigue fractured surfaces of MCBs and marked cracks with (a) $N_f = 63544$; (b) $N_f = 35045$ and (c) $N_f = 10328$.

creep compliance evolution of cement paste under constant loading can be determined by the combinations of rheological models or experimental data. In this study, the power-law function suggested in [35,89–92] is used. The formulation of the BSP for a multistep viscoelastic strain ε_{ve} of cement paste reads:

$$\varepsilon_{ve}(\sigma,t) = \sum_{i=1}^{n}[\sigma(t_i) - \sigma(t_{i-1})]\left[\alpha\left(\frac{t-t_i}{t_1}\right)^{\beta}\right] \quad (6)$$

where $\sigma(t_i) - \sigma(t_{i-1})$ is the actual stress increment at time interval $(t_i - t_{i-1})$. The α and β are two creep parameters, where the inverse of α is the so-called creep modulus [89]. These two parameters may slightly differ

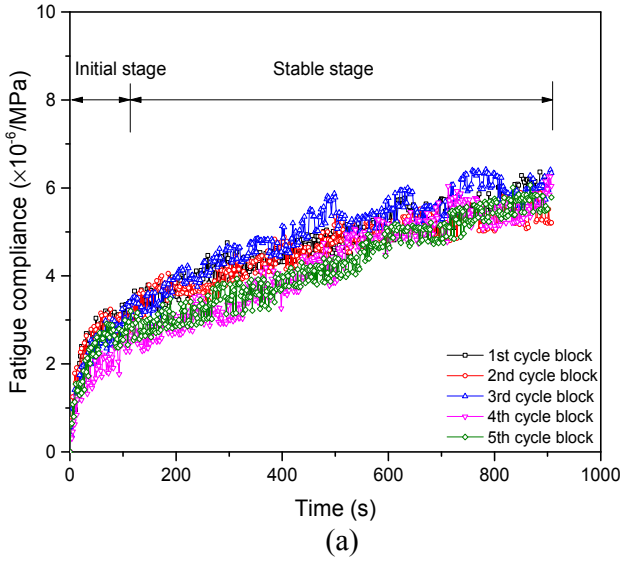

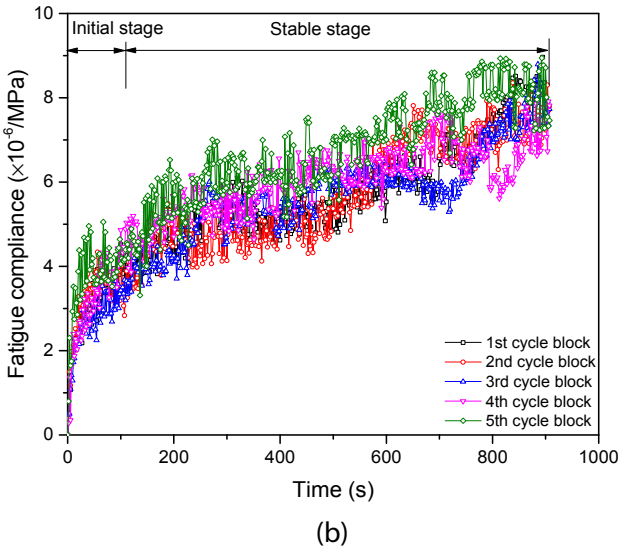

Fig. 20. The evolution of fatigue compliance for (a) w/c 0.4 and (b) w/c 0.5.

for each individual sample because of the heterogeneity of cement paste at the microscale. If the w/c 0.4 samples are considered here, the average creep parameters, which have been experimentally measured in author's previous work [39], are 1.47 and 0.203. After applying the real cyclic loading history (Fig. 5) into the equation, the viscoelastic deformation is obtained. Fig. 21 presents the comparison of fatigue compliance for w/c 0.4 samples, obtained from experiments and BSP based calculation. As can be seen in Fig. 21, the viscoelastic deformation based on BSP seems to account for most of the residual deformation of cement paste under cyclic loading especially at the first stage. With the increase of number of cycles, the viscoelastic deformation seems to still account for most of the measured fatigue compliance but a slight deviation from the experimental results is observed at the later stage. This deviation could be probably explained by the coupling between the fatigue crack growth and intrinsic viscoelastic deformation [9,83]. Overall, the major portion of the measured residual strain at the initial stage of fatigue loading can be attributed to the viscoelastic deformation of cement paste. In addition, the numerical work of Corrado and Molinari [26] indicates that the eigenstresses locally released around the cracks would induce a mismatch between the crack surfaces, which inhibits a perfect crack re-closure and contribute to the observed residual strain. However, their numerical results show that the simulated values of residual

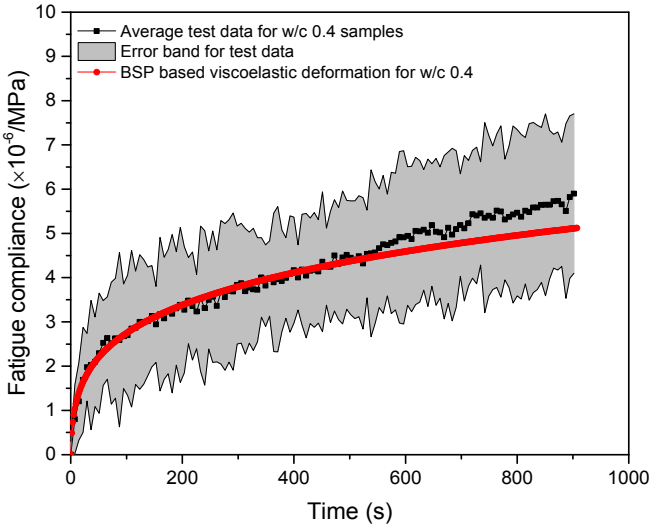

Fig. 21. The comparison of fatigue compliance curves for w/c 0.4 between test data and BSP based calculations.

deformation due to eigenstresses are only a small portion of the experimentally measured residual deformations. The possible concomitant effect of another mechanism suggested by the authors [26] is the formation of debris at a small scale, which may further prevent the crack closure [33]. Despite the complex deformation behaviour of cement paste in the second stage, the increase of the density of fatigue cracks and crack width along with the propagation of fatigue cracks are the main reasons for the development of residual fatigue compliance at the final stage.

4. Conclusions

In this research study, micro-cantilever cyclic bending tests have been performed to investigate the fatigue properties of cement paste at the microscale. The following conclusions can be drawn from the experimental results:

(1) Given the same stress level, the fatigue life of cement paste at the microscale is almost two orders of magnitude longer than that at the macroscale, indicating a strong size dependency of paste specimen.
(2) The microscopic fatigue damage evolution in cement paste is found to be very slow, indicated by the longer fatigue life as well as the less generated damage compared to the macroscopic fatigue of concrete.
(3) The fatigue damage accumulation in cement paste, in the forms of nano-scale crack propagations, is very small even under high stress levels (70–95%). When compared to the static fracture, a higher density of nano-scale cracks can be observed in fatigue fractured samples. Most of these cracks are the results of the fractured C-S-H phases, which are generally located at the stress concentrations. This suggests that, under fatigue loading, multiple nano-cracks propagate simultaneously inside the C-S-H gel particles and coalescence into a major crack before failure.
(4) Three distinct stages for the development of residual deformation can be identified. The residual deformation of cement paste measured at the microscale is not caused only by the fatigue cracking growth. Based on the linear viscoelasticity assumption, the viscoelastic deformation under cyclic loading seems to account for most of the measured residual deformation, especially at the initial stage of fatigue test. At the later stage, the residual deformation could be explained by coupling of fatigue crack growth and viscoelastic deformation.

The knowledge regarding the fatigue properties of cement paste at the microscale will help to gain some insights on the fatigue behaviour of concrete. However, in order to fully understand this behaviour, the fatigue properties of other components in concrete, i.e. ITZ, also need to be studied.

Declaration of Competing Interest

The authors declare that they have no known competing financial interests or personal relationships that could have appeared to influence the work reported in this paper.

Acknowledgments

Yidong Gan, Yu Zhang and Yading Xu would like to acknowledge the funding supported by China Scholarship Council, China under grant number 201706130140, 201808320456 and 201708110187. Hongzhi Zhang acknowledges the financial support from the Taishan Scholar Foundation of Shandong Province, China under the grant number tsqn201909032. Mr. Arjan Thijssen is also gratefully acknowledged for his help with the ESEM and XCT experiments.

References

[1] Keerthana K, Chandra Kishen JM. An experimental and analytical study on fatigue damage in concrete under variable amplitude loading. Int J Fatigue 2018;111:278–88.
[2] Kim JK, Kim YY. Experimental study of the fatigue behavior of high strength concrete. Cem Concr Res 1996;26:1513–23.
[3] Qiu J, Yang E. Micromechanics-based investigation of fatigue deterioration of engineered cementitious composite (ECC). Cem Concr Res 2017;95:65–74.
[4] Li Q, Huang B, Xu S, Zhou B, Yu RC. Compressive fatigue damage and failure mechanism of fiber reinforced cementitious material with high ductility. Cem Concr Res 2016;90:174–83.
[5] Gaedicke C, Roesler J, Shah S. Fatigue crack growth prediction in concrete slabs. Int J Fatigue 2009;31:1309–17.
[6] Wang XH, Bastidas-Arteaga E, Gao Y. Probabilistic analysis of chloride penetration in reinforced concrete subjected to pre-exposure static and fatigue loading and wetting-drying cycles. Eng Fail Anal 2018;84:205–19.
[7] Fu C, Ye H, Jin X, Yan D, Jin N, Peng Z. Chloride penetration into concrete damaged by uniaxial tensile fatigue loading. Constr Build Mater 2016;125:714–23.
[8] Hsu TTC. Fatigue and microcracking of concrete. Matériaux Constr 1984;17:51–4.
[9] Gao L, Hsu CTT. Fatigue of concrete under uniaxial compression cyclic loading. ACI Mater J 1998;95:575–81.
[10] Hsu TTC. Fatigue of Plain Concrete. ACI J Proc 1981;78:292–304.
[11] Simon KM, Chandra Kishen JM. A multiscale approach for modeling fatigue crack growth in concrete. Int J Fatigue 2017;98:1–13.
[12] Pichler C, Lackner R. Identification of logarithmic-type creep of calcium-silicate-hydrates by means of nanoindentation. Strain 2009;45:17–25.
[13] Van Breugel K. Concrete: A material that barely deserves that qualification, in: Int. RILEM Conf. Mater. Sci., RILEM Publications SARL; 2010: pp. 13–32.
[14] Le J-L, Bažant ZP. Unified nano-mechanics based probabilistic theory of quasibrittle and brittle structures: II. Fatigue crack growth, lifetime and scaling. J Mech Phys Solids 2011;59:1322–37.
[15] Sohel KMA, Al-Jabri K, Zhang MH, Liew JYR. Flexural fatigue behavior of ultra-lightweight cement composite and high strength lightweight aggregate concrete. Constr Build Mater 2018;173:90–100.
[16] Ding Z, Feng DC, Ren X, Wang J. Physically based constitutive modeling of concrete fatigue and practical numerical method for cyclic loading simulation. Eng Fail Anal 2019;101:230–42.
[17] Arora S, Singh SP. Fatigue strength and failure probability of concrete made with RCA. Mag Concr Res 2017;69:55–67.
[18] Lee MK, Barr BIG. An overview of the fatigue behaviour of plain and fibre reinforced concrete. Cem Concr Compos 2004;26:299–305.
[19] Müller S, Mechtcherine V. Fatigue behaviour of strain-hardening cement-based composites (SHCC). Cem Concr Res 2017;92:75–83.
[20] Ortega JJ, Ruiz G, Yu RC, Afanador-García N, Tarifa M, Poveda E, et al. Number of tests and corresponding error in concrete fatigue. Int J Fatigue 2018;116:210–9.
[21] Le J-L, Bažant ZP, Bazant MZ. Unified nano-mechanics based probabilistic theory of quasibrittle and brittle structures: I. Strength, static crack growth, lifetime and scaling. J Mech Phys Solids 2011;59:1291–321.
[22] Le JL, Manning J, Labuz JF. Scaling of fatigue crack growth in rock. Int J Rock Mech Min Sci 2014;72:71–9.
[23] Basquin OH. The exponential law of endurance tests. In: Proc Am Soc Test Mater; (1910) 625–630.
[24] Guo LP, Carpinteri A, Roncella R, Spagnoli A, Sun W, Vantadori S. Fatigue damage of high performance concrete through a 2D mesoscopic lattice model. Comput Mater Sci 2009;44:1098–106.
[25] Gong F, Ueda T, Wang Y, Zhang D, Wang Z. Mesoscale simulation of fatigue behavior of concrete materials damaged by freeze-thaw cycles. Constr Build Mater 2017;144:702–16.
[26] Corrado M, Molinari JF. Effects of residual stresses on the tensile fatigue behavior of concrete. Cem Concr Res 2016;89:206–19.
[27] Matsumoto K, Sato Y, Ueda T, Wang L. Mesoscopic analysis of mortar under high-stress creep and low-cycle fatigue loading. J Adv Concr Technol 2008;6:337–52.
[28] Toumi A, Bascoul A, Turatsinze A. Crack propagation in concrete subjected to flexural- cyclic loading. Mater Struct 1998;31:451–8.
[29] Simon KM, Kishen JMC. Influence of aggregate bridging on the fatigue behavior of concrete. Int J Fatigue 2016;90:200–9.
[30] Saito M. Characteristics of microcracking in concrete under static and repeated tensile loading. Cem Concr Res 1987;17:211–8.
[31] Zhang J, Li VC, Stang H. Size effect on fatigue in bending of concrete. J Mater Civ Eng 2001;13:446–53.
[32] Thomas Lee, T. The Effects of Air Content, Water-Cement Ratio and Aggregate Type on the Flexural Fatigue Strenght of Plain Concrete, Theses Diss, Ames: Iowa State University; (1979) 142–148.
[33] Grassl P, Rempling R. A damage-plasticity interface approach to the meso-scale modelling of concrete subjected to cyclic compressive loading. Eng Fract Mech 2008;75:4804–18.
[34] Gan Y, Zhang H, Šavija B, Schlangen E, van Breugel K. Static and fatigue tests on cementitious cantilever beams using nanoindenter. Micromachines 2018;9:1–15.
[35] Gan Y, Vandamme M, Zhang H, Chen Y, Schlangen E, van Breugel K, et al. Micro-cantilever testing on the short-term creep behaviour of cement paste at micro-scale. Cem Concr Res 2020;134:1–26.
[36] Zhang H, Gan Y, Xu Y, Zhang S, Schlangen E, Šavija B. Experimentally informed fracture modelling of interfacial transition zone at micro-scale. Cem Concr Compos 2019;104:1–12.
[37] Zhang J, Scherer GW. Comparison of methods for arresting hydration of cement. Cem Concr Res 2011;41:1024–36.
[38] Cowper GR. The Shear Coefficient in Timoshenko's Beam Theory. J Appl Mech 1966;33:335.
[39] Gan Y, Vandamme M, Chen Y, Schlangen E, van Breugel K, Šavija B. Experimental investigation of creep recovery of cement paste at the microscale, Cem Concr Res (submitted for publication).
[40] Chen X, Bu J, Fan X, Lu J, Xu L. Effect of loading frequency and stress level on low cycle fatigue behavior of plain concrete in direct tension. Constr Build Mater 2017;133:367–75.
[41] Saito M, Ishimori H. Chloride permeability of concrete under static and repeated compressive loading. Cem Concr Res 1995;25:803–8.
[42] Jiang C, Huang Q, Gu X, Zhang W. Experimental investigation on carbonation in fatigue-damaged concrete. Cem Concr Res 2017;99:38–52.
[43] Tait RB. Fatigue and fracture of cement mortar. PhD thesis. Johannesburg: University of Cape Town; 1984.
[44] E.O.L. Lantsoght, Fatigue of concrete under compression: Database and proposal for high strength concrete, Rep. Nr. 25.5-14-04. Delft University of Technology (2014).
[45] Vicente MA, González DC, Mínguez J, Tarifa MA, Ruiz G, Hindi R. Influence of the pore morphology of high strength concrete on its fatigue life. Int J Fatigue 2018;112:106–16.
[46] Vicente MA, Ruiz G, Gonzalez DC, Minguez J, Tarifa M, Zhang X. CT-Scan study of crack patterns of fiber-reinforced concrete loaded monotonically and under low-cycle fatigue. Int J Fatigue 2018;114:138–47.
[47] Zhang H, Šavija B, Figueiredo SC, Lukovic M, Schlangen E. Microscale testing and modelling of cement paste as basis for multi-scale modelling. Materials (Basel) 2016;9:1–14.
[48] Guang Y. Experimental Study and Numerical Simulation of the Development of the Microstructure and Permeability of Cementitious Materials. PhD thesis. Delft: Delft University of Technology; 2003.
[49] Zhang B, Phillips DV, Wu K. Effects of loading frequency and stress reversal on fatigue life of plain concrete. Mag Concr Res 1996;48:361–75.
[50] Zhaoxia L, Yaoping H. Effect of strain rate on the compressive strength surface cracking and failure mode of mortar. ACI Mater J 1998;95:512–8.
[51] Fischer I, Pichler B, Lach E, Terner C, Barraud E, Britz F. Compressive strength of cement paste as a function of loading rate: Experiments and engineering mechanics analysis. Cem Concr Res 2014;58:186–200.
[52] Gan Y, Rodriguez CR, Schlangen E, van Breugel K, Šavija B. Assessing strain rate sensitivity of cement paste at the micro-scale through micro-cantilever testing. Cem Concr Compos 2021;121:1–12.
[53] Vegt I. Concrete in dynamic tension: the fracture process. PhD thesis. Delft: Delft University of Technology; 2016.
[54] Kirane K, Bažant ZP. Size effect in Paris law and fatigue lifetimes for quasibrittle materials: Modified theory, experiments and micro-modeling. Int J Fatigue 2016;83:209–20.
[55] Bazant ZP, Xu K. Size effect in fatigue fracture of concrete. ACI Mater J 1991;88:390–9.
[56] Bazant ZP, Schell WF. Fatigue fracture of high-strength concrete and size effect. ACI Mater J 1993;90:472.
[57] Carpinteri A, Spagnoli A, Vantadori S. An approach to size effect in fatigue of metals using fractal theories. Fatigue Fract Eng Mater Struct 2002;25:619–27.
[58] Carpinteri A, Spagnoli A, Vantadori S. Size effect in S – N curves: A fractal approach to finite-life fatigue strength. Int J Fatigue 2009;31:927–33.
[59] Carpinteri A, Spagnoli A. A fractal analysis of size effect on fatigue crack growth. Int J Fatigue 2004;26:125–33.

[60] Carpinteri A, Spagnoli A, Vantadori S. A multifractal analysis of fatigue crack growth and its application to concrete. Eng Fract Mech 2010;77:974–84.
[61] Raju NK. Comparative Study of the Fatigue Behavior of Concrete, Mortar, and Paste in uniaxial compression. J Proc 1970:461–3.
[62] Antrim JD. The mechanism of fatigue in cement paste and plain concrete. In: A Symp Concr Strength; 5 Reports; 1967. p. 95–107.
[63] Alliche A, François D. Fatigue behavior of hardened cement paste. Cem Concr Res 1986;16:199–206.
[64] Morris AD, Garrett GG. A comparative study of the static and fatigue behaviour of plain and steel fibre reinforced mortar in compression and direct tension. Int J Cem Compos Light Concr 1981;3:73–91.
[65] Murdock JW. A critical review of research on fatigue of plain concrete. Univ Illinois Eng Exp Stn Bull 1965:25.
[66] Oneschkow N. Fatigue behaviour of high-strength concrete with respect to strain and stiffness. Int J Fatigue 2016;87:38–49.
[67] Bindiganavile V, Banthia N. Size effects and the dynamic response of plain concrete. J Mater Civ Eng 2006;18:485–91.
[68] Bazant ZP, Planas J. Fracture and size effect in concrete and other quasibrittle materials. CRC Press; 1997.
[69] Anderson KV, Daniewicz SR. Statistical analysis of the influence of defects on fatigue life using a Gumbel distribution. Int J Fatigue 2018;112:78–83.
[70] Zhang B. Relationship between pore structure and mechanical properties of ordinary concrete under bending fatigue. Cem Concr Res 1998;28:699–711.
[71] Fan Z, Sun Y. Detecting and evaluation of fatigue damage in concrete with industrial computed tomography technology. Constr Build Mater 2019;223:794–805.
[72] Isojeh B, El-Zeghayar M, Vecchio FJ. Concrete damage under fatigue loading in uniaxial compression. ACI Mater J 2017;114:225–35.
[73] Awad ME. Strength and deformation characteristics of plain concrete subjected to high repeated and sustained loads. University of Illinois Engineering Experiment Station. College of Engineering. University of Illinois at Urbana-Champaign; 1971.
[74] Huang Y, Yang Z, Ren W, Liu G, Zhang C. 3D meso-scale fracture modelling and validation of concrete based on in-situ X-ray Computed Tomography images using damage plasticity model. Int J Solids Struct 2015;67–68:340–52.
[75] Obara Y, Tanikura I, Jung J, Shintani R, Watanabe S. Evaluation of Micro-damage of Concrete Specimens under Cyclic Uniaxial Loading by X-ray CT Method. J Adv Concr Technol 2016;14:433–43.
[76] Cao J, Chung DDL. Minor damage of cement mortar during cyclic compression monitored by electrical resistivity measurement. Cem Concr Res 2001;31:1519–21.
[77] Zhang H, Rodriguez CR, Dong H, Gan Y, Schlangen E, Šavija B. Elucidating the effect of accelerated carbonation on porosity and mechanical properties of hydrated Portland cement paste using X-ray tomography and advanced micromechanical testing. Micromachines 2020;11:1–14.
[78] Suaris W, Fernando V. Ultrasonic Pulse Attenuation As a Measure of Damage Growth During Cyclic Loading of Concrete. ACI Mater J 1987;84:185–93.
[79] Susmel L. A unifying methodology to design un-notched plain and short-fibre/particle reinforced concretes against fatigue. Int J Fatigue 2014;61:226–43.
[80] Lemaitre J, Desmorat R. Background on continuum damage mechanics. In: Eng. Damage Mech. Ductile, Creep, Fatigue Brittle Fail; 2005. p. 1–76.
[81] Leckie F. A course on damage mechanics, Springer Science & Business Media; 1998.
[82] Jiang L, Li C, Zhu C, Song Z, Chu H. The effect of tensile fatigue on chloride ion diffusion in concrete. Constr Build Mater 2017;151:119–26.
[83] Bazant ZP, Hubler MH. Theory of cyclic creep of concrete based on Paris law for fatigue growth of subcritical microcracks. J Mech Phys Solids 2014;63:187–200.
[84] Suwanmaneechot P, Aili A, Maruyama I. Creep behavior of C-S-H under different drying relative humidities: Interpretation of microindentation tests and sorption measurements by multi-scale analysis. Cem Concr Res 2020;132:1–13.
[85] Wyrzykowski M, Gajewicz-Jaromin AM, McDonald PJ, Dunstan DJ, Scrivener KL, Lura P. Water Redistribution-Microdiffusion in Cement Paste under Mechanical Loading Evidenced by 1H NMR. J Phys Chem C 2019;123:16153–63.
[86] Alizadeh R, Beaudoin JJ, Raki L. Viscoelastic nature of calcium silicate hydrate. Cem Concr Compos 2010;32:369–76.
[87] Vandamme M, Ulm FJ. Nanoindentation investigation of creep properties of calcium silicate hydrates. Cem Concr Res 2013;52:38–52.
[88] Gurtin ME, Sternberg E. On the linear theory of viscoelasticity. Arch Ration Mech Anal 1961;7:402–11.
[89] Irfan-Ul-Hassan M, Pichler B, Reihsner R, Hellmich C. Elastic and creep properties of young cement paste, as determined from hourly repeated minute-long quasi-static tests. Cem Concr Res 2016;82:36–49.
[90] Tamtsia BT, Beaudoin JJ. Basic creep of hardened cement paste. A re-examination of the role of water. Cem Concr Res 2000;30:1465–75.
[91] Van Breugel, K. Relaxation of young concrete, Report. Delft University of Technology; (1980) 144.
[92] Gan Y, Rodriguez C, Zhang H, Schlangen E, van Breugel K, Šavija B. Modeling of microstructural effects on the creep of hardened cement paste using an experimentally informed lattice model. Comput Civ Infrastruct Eng 2021:1–17.